Lawrence Berkeley National Laboratory

Title
Impact of UV-induced ozone and low-energy Ar+-ion cleaning on the chemical structure of Cu(In,Ga)(S,Se)2 absorber surfaces

Permalink
https://escholarship.org/uc/item/9sg222sr

Authors
van Maris, Victor R
Hauschild, Dirk
Niesen, Thomas P
et al.

Peer reviewed

Impact of UV-induced Ozone and Low-Energy Ar+-Ion Cleaning on the Chemical Structure of Cu(In,Ga)(S,Se)₂ Absorber Surfaces

Victor R. van Maris[1,2], Dirk Hauschild[1,2,3,*], Thomas P. Niesen[4], Patrick Eraerds[4], Thomas Dalibor[4], Jörg Palm[4], Monika Blum[5,6], Wanli Yang[5], Clemens Heske[1,2,3], and Lothar Weinhardt[1,2,3,*]

[1]Institute for Photon Science and Synchrotron Radiation (IPS), Karlsruhe Institute of Technology (KIT), Hermann-v.-Helmholtz-Platz 1, 76344 Eggenstein-Leopoldshafen, Germany

[2]Institute for Chemical Technology and Polymer Chemistry (ITCP), Karlsruhe Institute of Technology (KIT), Engesserstraße 18/20, 76131 Karlsruhe, Germany

[3]Department of Chemistry and Biochemistry, University of Nevada, Las Vegas (UNLV), 4505 Maryland Parkway, Las Vegas, NV 89154-4003, United States

[4]AVANCIS GmbH, Solarstraße 3, 04860 Torgau, Germany

[5]Advanced Light Source, Lawrence Berkeley National Laboratory, 1 Cyclotron Road, Berkeley, CA 94720, United States

[6]Chemical Sciences Division, Lawrence Berkeley National Laboratory, 1 Cyclotron Road, Berkeley, CA 94720, United States

*Authors to whom correspondence should be addressed:
dirk.hauschild@kit.edu, lothar.weinhardt@kit.edu

ABSTRACT

Dry buffer layer deposition techniques for chalcopyrite (CIGSSe)-based thin-film solar cells lack the surface-cleaning characteristics of the commonly used CdS or Zn(O,S) wet-chemical bath deposition. A UV-induced ozone and/or a low-energy Ar^+-ion treatment could provide dry CIGSSe surface cleaning steps. To study the impact of these treatments, the chemical surface structure of a CIGSSe absorber is investigated. For this purpose, a set of surface-sensitive spectroscopic methods, i.e., laboratory-based x-ray photoelectron spectroscopy and x-ray-excited Auger electron spectroscopy, is combined with synchrotron-based soft x-ray emission spectroscopy. After treatment times as short as fifteen seconds, the UV-induced ozone treatment decreases the amount of carbon adsorbates at the CIGSSe surface significantly, while the oxygen content increases. This is accompanied by the oxidation of all absorber surface elements, i.e., indium, selenium, sulfur, and copper. Short (60 s) low-energy Ar^+-ion treatments, in contrast, primarily remove oxygen from the surface. Longer treatment times also lead to a removal of carbon, while extremely long treatment times can also lead to additional (likely metallic) Cu phases at the absorber surface as well.

1. Introduction

Chalcopyrite-based thin-film solar cells and modules can be processed with different buffer layers, such as CdS or Zn(O,S) [by chemical bath deposition (CBD)] or In_2S_3 [by physical vapor deposition (PVD)]. Research and development of such buffer layers [e.g., Zn(O,S),[1–4] (Zn,Mg)O,[5,6] and In_2S_3[7–10]] is motivated by the replacement of Cd, the increase of efficiency by increasing the optical transmission, and/or the replacement of wet processes to improve the environmental footprint by avoiding waste water. Among the alternative approaches, atomic layer deposition,[11] ion layer gas reaction,[12] and PVD[13] have been prominently reported. Such "dry" processes, however, lack the surface-cleaning properties of the CBD, which may have a negative impact on the performance of the complete solar cell device. In fact, several studies have shown degradation effects of air-exposed co-evaporated $CuInSe_2$ or $Cu(In,Ga)Se_2$ absorbers on the minute and long-term time scale, leading to a reduction of the open circuit voltage (V_{OC}) in the full solar cell.[14,15] Surface studies have revealed the adsorption of, e.g., carbon hydroxides and water ("surface adsorbates"), the formation of oxides, and segregation as potential reason for this degradation.[16–20] In this work, the physical and chemical impact of two different dry treatments on the surface of $Cu(In,Ga)(S,Se)_2$ (CIGSSe) absorbers is investigated.

Possible candidates for dry cleaning treatments include a UV-induced ozone treatment and a low-energy (50 eV) Ar^+-ion surface treatment, which are both candidate treatments for inclusion in a dry in-line process. In the UV treatment, photoexcitation by a low-pressure mercury lamp generates ozone (O_3) from ambient oxygen, which is subsequently decomposed into (highly reactive) atomic oxygen. Hydrocarbons at the surface are excited and dissociated by a characteristic mercury line (253.7 nm), which makes it more likely for them to react with the atomic oxygen, creating volatile molecules (e.g., carbon oxides and hydroxides) that then desorb from the surface.[21–24] UV-induced ozone treatments are already used in production processes for other thin-film disciplines.[25,26] For indium-tin-oxide (ITO) thin films, it is reported that a UV treatment reduces the relative concentration of carbon atoms and forms a Sn-deficient and O-rich surface,[27] but other studies indicated "not much change" in the chemical composition.[28] In the soft x-ray synchrotron community, a UV treatment is commonly used to remove carbon adsorbates from beamline optics.[29]

In the low-energy (50 eV) Ar^+-ion treatment, a commercial ion gun is used at very low energies to stimulate adsorbate desorption with minimal (or no) sputter damage to the surface. This approach was first established by Weinhardt *et al.*[30] to remove adsorbates from CIGSSe surfaces without the

previously observed surface metallization by sputter-cleaning surfaces at 500 eV.[31,32] Most dominantly, sputtering at 500 eV (or above, as commonly used in destructive depth-profile approaches) led to preferential enrichment of CIGSSe surfaces with Cu, coupled with the creation of a metallic surface layer (as evidenced by the presence of a Fermi edge in UV and inverse photoemission spectra).

In this paper, a UV-induced ozone treatment and a low-energy Ar^+-ion treatment (including an ultra-long treatment experiment of 2 hours) is applied to CIGSSe-based absorber surfaces to study their impact on the chemical surface structure. For this purpose, x-ray photoelectron spectroscopy (XPS) and x-ray exited Auger electron spectroscopy (XAES) are used to examine CIGSSe surfaces after each treatment step. This measurement set is combined with soft x-ray emission spectroscopy (XES) to also give element-specific chemical structure information at and near the surface, but in a complementary fashion to XPS and XAES.[33]

2. Experimental Section

All samples originate from one 10 x 10 cm^2 absorber sample processed by AVANCIS GmbH using the R&D base line process.[34] The (air-exposed) sample was shipped to KIT, where the sample was transferred into an Argon-filled glovebox directly connected to the ultra-high vacuum surface characterization system (Materials for Energy – MFE lab at KIT, Scienta Omicron). Here, the 10 x 10 cm^2 sample was cut into several smaller pieces. Each piece was unloaded separately from the glovebox, put into a UV-induced ozone cleaner (UVO-Cleaner Model 18, Jelight Company Inc.), treated for a given duration (15, 45, 60, 75, 90, and 1200 s), and subsequently loaded back into the glovebox to minimize air exposure *after* the treatment. Note that, for industrial application in an in-line process, the use of a glovebox would not be required. The ambient air exposure time before and after the treatment was minimized to less than 10 seconds each. For the low-energy Ar^+-ion treatment, a FOCUS FDG 150 ion source was utilized (E_{ion} = 50 eV, j_{sample} ~300 nA/cm^2, treatment times of 60, 120, 180, 3600, and 7200 s) at an angle of 45° with respect to the sample normal. XPS and XAES were measured with a non-monochromatized DAR 450 twin anode x-ray source (Mg and Al K_α) and an Argus CU electron analyzer (Scienta Omicron), calibrated according to Moulder *et al*. using Au, Ag, and Cu metal references.[35] The base pressure was ~$1\cdot10^{-10}$ mbar in the analysis chamber.

After the XPS and XAES measurements, small pieces were cut off from the measured samples, sealed under inert atmosphere in the glovebox, and shipped to Beamline 8.0.1 of the Advanced Light Source

(ALS) in Berkeley for XES measurements (with brief air exposure during loading into the XES chamber). A CdS reference sample was used to calibrate the emission energy axis for the here-presented S $L_{2,3}$ XES spectra.[36]

3. Results and Discussion

In the XPS survey spectra (Fig. 1), all peaks associated with the absorber elements (copper, indium, sulfur, and selenium) are visible. Only trace amounts of gallium are detected at the absorber surface (accordingly, the surface is sometimes called "CISSe")[34,37,38]. In addition, sodium- (e.g., Na 1s), oxygen- (e.g., O 1s) and carbon-related (e.g., C 1s) signals can be identified. For the 7200 s Ar$^+$-ion treated sample, a small Ar 2p signal is found (at ~240 eV, not visible in Fig. 1). For the as-received sample (in the following "untreated"), the carbon and oxygen peaks are clearly visible, indicating that the sample exhibits a significant amount of surface adsorbates (as we will show in the following).
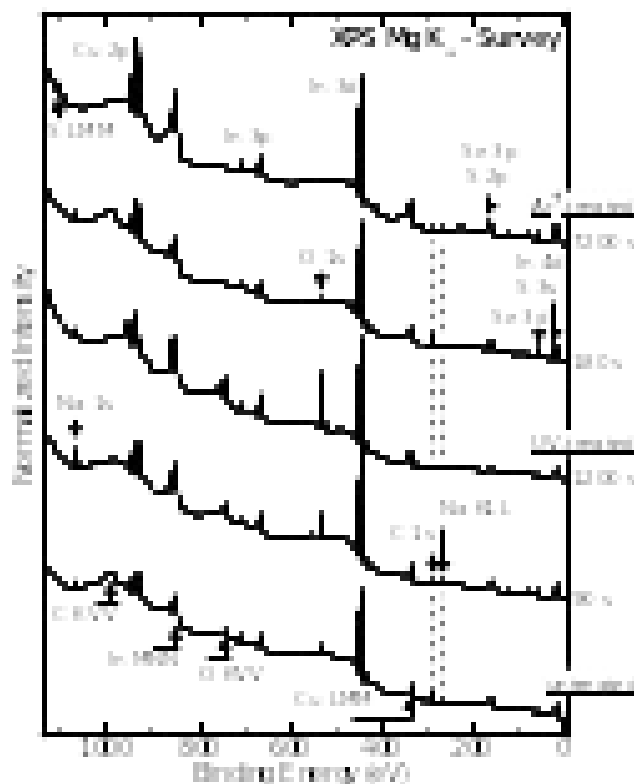

Fig. 1: Mg K$_\alpha$ XPS survey spectra of CIGSSe absorbers that underwent (from bottom to top): no treatment, 90 s UV treatment, 1200 s UV treatment, 180 s low-energy Ar$^+$-ion treatment, and 7200 s Ar$^+$-ion treatment. Prominent XPS and XAES signals are labeled.

As already visible in the survey spectra of Fig. 1, and more easily seen in the detail spectra of Fig. 2, the sample that underwent a 90 s UV-induced ozone treatment shows an intensity increase of the O 1s signal (×2.6), while that of C 1s is decreased (÷3.0). The increase in the oxygen signal can be attributed to the formation of metal oxides and hydroxides, which causes a shift of the peak maximum to lower binding energies (indicated by the grey dashed line in Fig. 2). The reduction of the carbon signal is primarily associated with the main C 1s contribution (amorphous carbon and hydrocarbons), while the (much smaller) carbonates/carboxyl component is not significantly altered.

In addition, all absorber-related lines (including Na 1s) become more intense due to the lower attenuation at the absorber surface. For longer UV-treatment times (1200 s), the O 1s peak is further increased, and only a very small C 1s intensity remains. In parallel, the Cu Auger feature is broadened and the spectral shape of the Cu 2p signal is significantly changed, indicating a different chemical environment (which will be discussed later), and the Na 1s peak is reduced in intensity. Most likely, volatile sodium-containing components are formed under the UV light, e.g., with participation of H_2O molecules, similar to a rinsing step.[17,39] We also observe that the intensity decrease of the less surface-sensitive Na KLL Auger line is even more pronounced than that of the Na 1s, which rules out a possible attenuation of the signals by adsorbate layers, and indicates that Na is still localized at the topmost layer of the film after the prolonged UV treatment.

For the *Ar$^+$-ion treated* samples, the O 1s signal is strongly reduced, even for short treatment times (180 s), while the C 1s intensity is reduced slightly. Only significantly longer treatment times (3600 and 7200 s) are able to reduce the concentration of all *carbon*-containing species from the surface (by a factor of ~4). Furthermore, sodium is almost completely removed, suggesting that sodium is only present at the outermost surface.[39,43] The removal of C, O, and Na leads to higher intensities of all absorber photoemission lines (due to reduced signal attenuation).
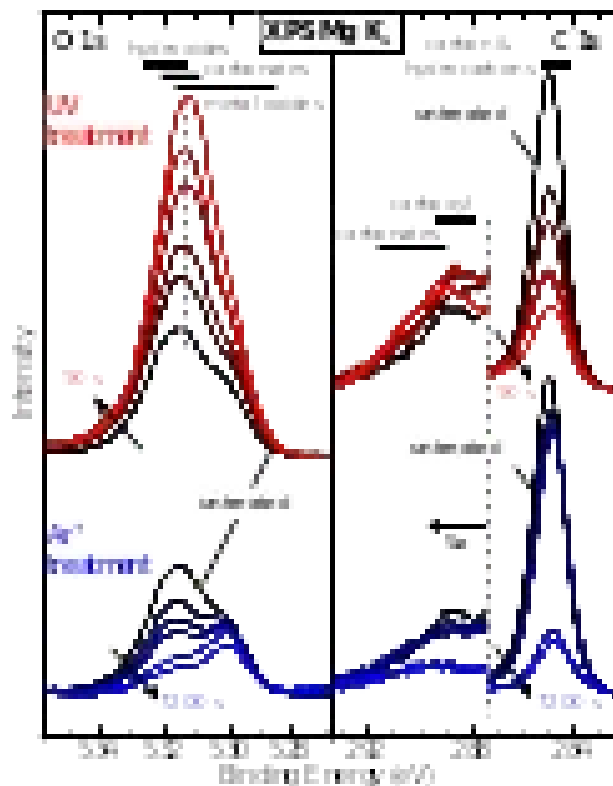
Fig. 2: Mg K$_\alpha$ XPS spectra of the O 1s (left) and C 1s (right) regions for the untreated (black), UV-treated (15, 45, 60, 75, 90 s; from black to red), and Ar$^+$-ion treated (60, 120, 180, 3600, 7200 s; from black to blue) surfaces. The ordinate is given as an "intensity-true" representation, allowing for a direct comparison of the spectral area under the curves. Black bars indicate chemical species commonly found for C and O adsorbates.[35,40–42] Arrows serve as a guide-to-the-eye for the spectral evolution, and a dashed line for the O 1s peaks after UV treatment is used to illustrate a shift to lower binding energy.

The evolution of the oxygen 1s line during the Ar$^+$-ion treatment reveals multiple components. The analysis of absorber elements, discussed later, will show In-O and Se-O bonds, and some surface adsorbates (water, hydroxides) are likely present (and removed) as well. The largest contribution is removed during the first treatment step. We note that the concentration of physisorbed species could also be reduced by an annealing step; however, this runs the risk of also inducing annealing-related changes in the surface-near bulk of the absorber (e.g., the Cu profile).
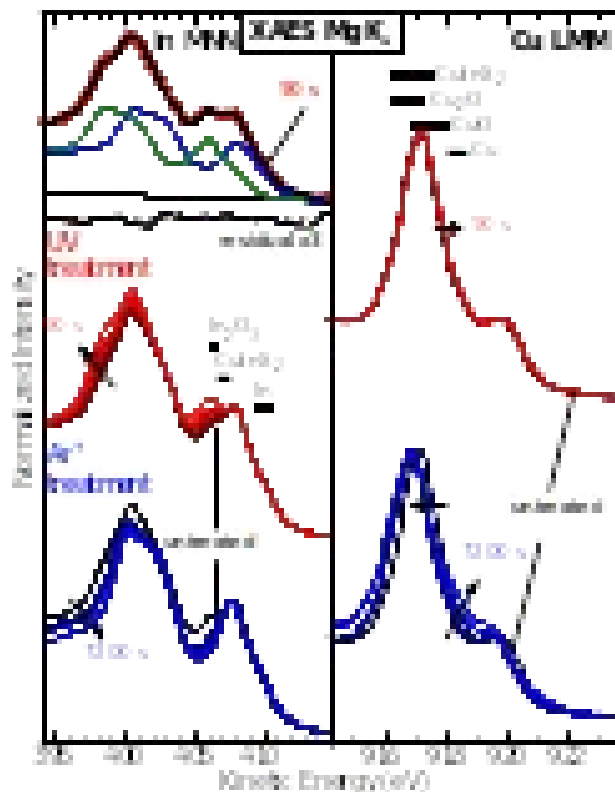
Fig. 3: Mg K$_\alpha$ XAES spectra of the In M$_{4,5}$N$_{4,5}$N$_{4,5}$ (left) and Cu L$_3$M$_{4,5}$M$_{4,5}$ (right) Auger features for the untreated (black), UV-treated (15, 45, 60, 75, 90 s; from black to red), and Ar$^+$-ion treated (60, 120, 180, 3600, 7200 s; from black to blue) surfaces. The In spectra were normalized to the M$_4$N$_{4,5}$N$_{4,5}$ peak at ~408 eV, while the Cu spectra were normalized to the L$_3$M$_{4,5}$M$_{4,5}$ peak at ~917 eV. A fits of the In Auger feature for the 90 s UV-treated sample is also shown (top left).

To study the impact of the treatments on the CIGSSe absorber elements, we next analyze the In M$_{4,5}$N$_{4,5}$N$_{4,5}$ and Cu L$_3$M$_{4,5}$M$_{4,5}$ Auger features (Fig. 3). The indium Auger feature for the untreated sample already shows some indium-oxygen bonds, recognizable by the additional intensity in the "valley" at ~405 eV. The UV treatment further increases the amount of oxidized indium. For the 90 s UV-treated sample, the spectrum can be fitted by two In MNN components. The first (non-oxidized) spectral component is described by the spectrum after 7200 s of Ar$^+$-ion treatment, while the second component is represented by the same spectrum, but shifted by 2.1 eV to lower kinetic energy to emulate indium oxide. We note that the In MNN Auger transition only involves 3d and 'shallow' 4d core levels, resulting in very similar In MNN line shapes for different compounds. The indium oxide component in the 90 s UV-treated sample accounts for 50 % (± 2 %) of the overall In signal. From the

8

energetic position of the $M_4N_{4,5}N_{4,5}$ peak, and the modified In Auger parameter (851.5 ± 0.1 eV), it can be concluded that this second component indeed represents In-O bonds. In contrast, the Ar⁺-ion treatment completely removes the indium-oxygen bonds, best seen in the deepening of the valley at ~405 eV. For the 7200 s Ar⁺-ion treated sample, only one (non-metallic) In species is visible in the In MNN spectrum.
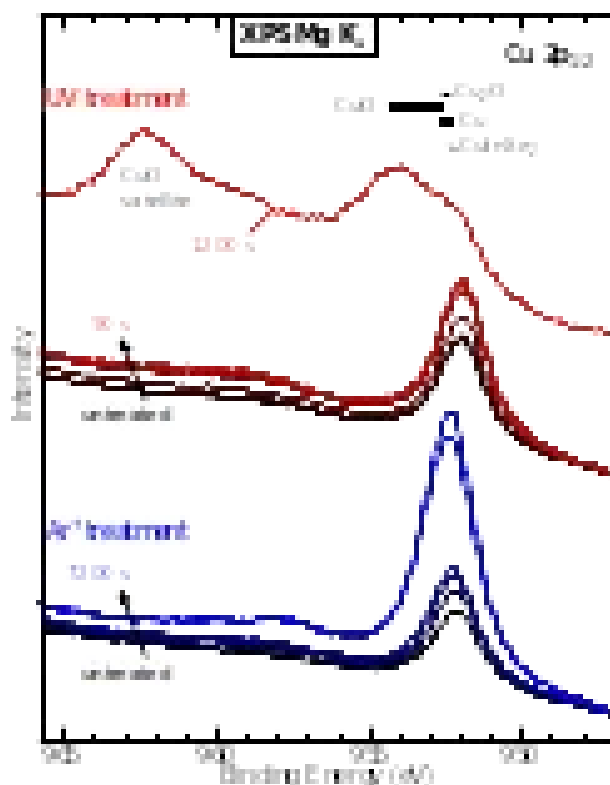

Fig. 4: Mg K_α XPS spectra of the Cu $2p_{1/2}$ region for the untreated (black), UV-treated (15, 45, 60, 75, 90, 1200 s, from black to red), and Ar⁺-ion treated (60, 120, 180, 3600, 7200 s; from black to blue) surfaces. The ordinate is given as an "intensity-true" representation, allowing for a direct comparison of the spectral area under the curves. Black bars indicate chemical species commonly found for Cu $2p_{1/2}$.[42] Arrows serve as guide-to-the-eye for the spectral evolution.

In the case of the Cu LMM Auger transitions, UV treatments up to 90 s only lead to a small shift to higher kinetic energy. Likewise, the corresponding Cu $2p_{1/2}$ spectra in Fig. 4 do not show a change in spectral shape [but an increase in overall intensity, due to the high surface-sensitivity (low kinetic energy) of the electrons contributing to the Cu 2p signal and the reduction of surface adsorbates]. For longer UV treatment times (1200 s; top spectrum in Fig 4), in contrast, the Cu $2p_{1/2}$ spectral shape

changes significantly and now includes a strong satellite feature (at ~962.5 eV) that can be ascribed to the formation of CuO.[44]

Upon Ar$^+$-ion treatment, the Cu LMM spectra in Fig. 3 shift to lower kinetic energies, and, for longer treatment times, the valley at 919 eV gets less pronounced. In the spectrum of the 7200 s Ar$^+$-ion treated sample, a clear contribution of a second component can be seen. Likewise, shifts to higher binding energy and a line broadening are observed in the Cu 2p$_{1/2}$ spectra. We speculate that this is due to Cu atoms in a metallic Cu environment.[45] While the creation of metallic surface species (in particular Cu, due to preferential sputtering of the other elements in CIGSSe) is a known effect when using higher energies and/or longer sputter times,[31,46] it is here observed for the first time when using 50 eV Ar$^+$ ions. However, we point out that this is related to the exceedingly long ion-treatment time and rather high current densities. Typically, short treatments (such as the 90 s employed here) are fully sufficient to remove the majority of "removable" surface contaminants, without any evidence of metallic copper (or other metallic components) in XPS, XAES, UV photoelectron spectroscopy (UPS), and inverse photoemission spectroscopy (IPES).
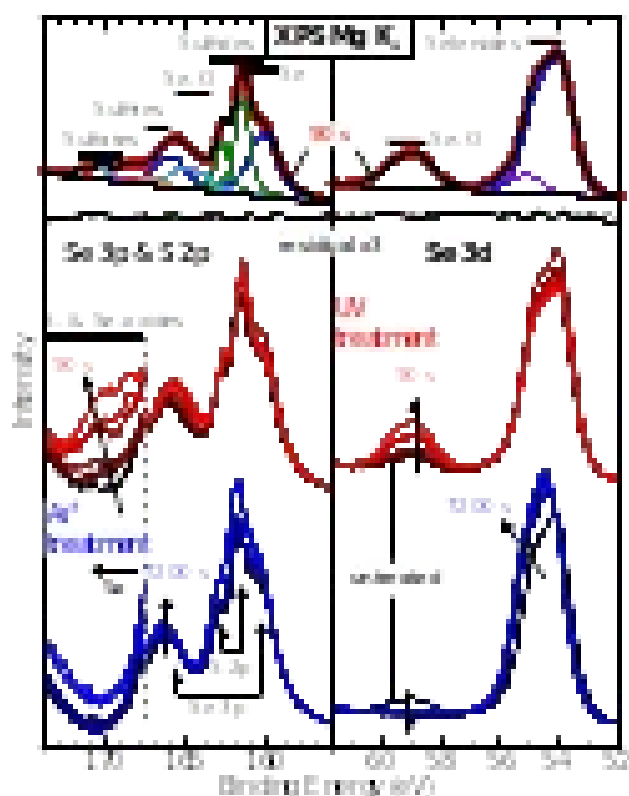
Fig. 5: Mg K$_\alpha$ XPS spectra of the Se 3p / S 2p (left) and the Se 3d (right) region for the untreated (black), UV-treated (15, 45, 60, 75, 90 s; from black to red), and Ar$^+$-ion treated (60, 120, 180, 3600, 7200 s; from black to blue) surfaces. The ordinate is given as an "intensity-true" representation, allowing for a direct comparison of the spectral area under the curves. At the top, fits of the Se 3p / S 2p (left) and Se 3d (right) region of the 90 s UV-treated sample are shown.

In addition to the copper and indium signals, the absorber constituents sulfur and selenium were analyzed, in particular the Se 3p / S 2p and Se 3d regions (Fig. 5). The untreated Se 3d spectrum consists of the chalcopyrite main feature at ~54 eV and a second feature at ~59 eV, which is increasing for increasing UV-treatment times. For longer UV-treatment times (75 s), additional intensity is found at ~55 eV, suggesting a third Se component. In order to separate the individual components, the 90 s UV-treated sample was fitted with a minimal number of spin-orbit-split Voigt doublets (three). The Gaussian and Lorentzian contributions were fixed for each individual component, the area ratio was kept constant at 3:2 according to the 2j+1 multiplicity, and the spin-orbit splitting was set to 0.86 eV. The first component at ~54 eV can be assigned to Se in a selenide environment (e.g., CISSe); the second one at ~55 eV could indicate a second selenide (e.g., Cu-Se bonds) or elemental Se; also, an inhomogeneous distribution of slightly varying local environments appears possible. The third component (at ~59 eV) exhibits a shift of ~4.7 eV with respect to the main component, suggesting Se-O bonds (as already observed for the untreated sample). The Ar$^+$-ion treatment fully removes the Se-O component already after the first 60 s treatment. In parallel, the intensity of the main component increases due to reduced amount of surface adsorbates.

Due to the spectral overlap, the Se 3p / S 2p core level region shows a complex behavior upon the UV treatment. Additional intensity is found in the valley between the S 2p and Se 3p$_{1/2}$ peak at ~165 eV, and the spectral intensity between 168 and 173 eV increases. To analyze these signals, the 90 s UV-treated spectrum was fitted with a Se 3p doublet (blue; for the Se component in a CISSe environment), a second Se doublet (light blue; for the Se-O component as identified from the Se 3d signal), and three S 2p doublets. Note that the Se 3d analysis shows the presence of a third Se species, but due to the overlap with the S 2p signals and the larger widths of the Se 3 p lines, the Se 3p / S 2p region can be sufficiently well described with only two spectral Se components. For each doublet, two Voigt profiles (Gaussian:Lorentzian ratio fixed, area ratio 2:1, spin-orbit splitting set to 1.2 and 5.7 eV for S 2p and Se 3p, respectively) were used. This approach results in one sulfide- (at 161.6 eV, green) and two S-O-

related signals (at 167.4 and 168.6 eV, orange and pink, resp.). The two additional S-O signals can be assigned to sulfites and sulfates, for which more evidence will be presented in the XES results below.

In contrast, the Ar^{+}-ion treatment does not modify the Se 3p / S 2p region significantly. The main effect is an overall intensity increase, which can, again, be related to the reduced attenuation of the XPS signal due to the removal of surface adsorbates.
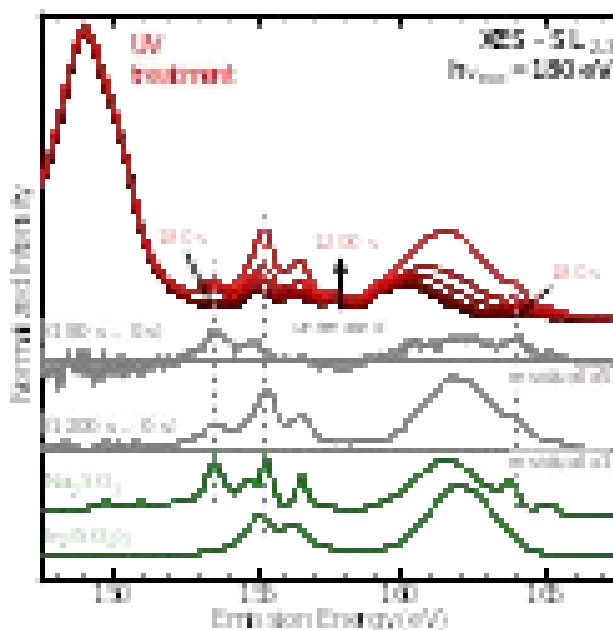

Fig. 6: S $L_{2,3}$ XES spectra ($h\nu_{excitation}$ = 180 eV) of the untreated CIGSSe absorber surface (black) and after different UV-treatment times (60, 120, 180, 300, 600, and 1200 s; from black to red), difference spectra (180 s – 0 s) and (1200 s - 0 s), and Na_2SO_3 and $In_2(SO_4)_3$ reference spectra.

To derive chemical information with an increased information depth, X-ray emission spectroscopy (XES) measurements at the S $L_{2,3}$ edge are presented in Fig. 6. Using the element-specific and local nature of XES, the S $L_{2,3}$ emission gives detailed information of the local chemical environment of sulfur in a complementary fashion to XPS. All spectra are dominated by the S 3s → S 2p emission at 149 eV, typical for a sulfide environment[47]. For the untreated sample (black), the spectral structure between 154 and 158 eV can be assigned to In 5s-derived bands, indicating S-In bonds. The broad signal at ~160.5 eV originates from Cu 3d-derived bands, indicating S-Cu bonds. For increasing UV-treatment time, several new features appear, e.g., at 153.5 and 164.0 eV. A difference spectrum of the 180 s UV-treated sample and the 0 s (untreated) sample highlights additional spectral weight between 160 and 164

eV. A comparison with Na_2SO_3 and $In_2(SO_4)_3$ reference spectra suggests the formation of sulfur-oxygen bonds, best described as a sulfite (SO_3^{2-}). For longer UV-treatment times, additional features at 155.3 and 156.5 eV and a broad maximum at ~162 eV become more pronounced. The difference spectrum (1200 s – 0 s) strongly resembles the reference spectrum of a sulfate, with an admixture of the sulfite spectra features. Note that the Na_2SO_3 and $In_2(SO_4)_3$ reference spectra are only used to demonstrate the most pertinent sulfite and sulfate features - the formation of other sulfates and sulfites is also possible. Nevertheless, the finding of both sulfite as well as sulfate spectral features supports the XPS findings of two distinct S-O bond signals in Fig. 5. The UV-induced ozone treatment hence clearly produces S-O bonds with varying degrees of oxidation.

4. Summary and Conclusion

The impact of two dry surface-cleaning approaches for CIGSSe solar cell absorbers, namely a UV-induced ozone treatment and a low-energy (50 eV) Ar^+-ion treatment were investigated for different treatment times. Even for UV treatments as short as 90 s, we find a two-thirds reduction of carbon and hydrocarbons but also an increase of oxygen at the CIGSSe absorber surface. This is accompanied by an oxide formation of indium, selenium, and sulfur after several tens of seconds at the surface. Copper remains unaffected for the first three minutes of the UV treatment, but also shows oxidized components when treated for 20 minutes. Furthermore, sulfite and sulfate signatures are found. In contrast, the low-energy Ar^+-ion treatment readily removes surface oxygen species, while longer treatment times also lead to a removal of carbon. For very long treatment times, metallic surface phases are also induced. As both treatments appear very effective, already for short treatment times (i.e., carbon removal for UV treatment and oxygen removal for low-energy ion treatment), we speculate that a sequential execution might represent a promising pathway to minimize carbon and oxygen surface contaminants for optimized heterojunction engineering in high-efficiency thin-film solar cells.

DATA AVAILABILITY STATEMENT

The data that support the findings of this study are available from the corresponding author upon reasonable request.

REFERENCES

[1] M. Mezher, R. Garris, L.M. Mansfield, M. Blum, D. Hauschild, K. Horsley, D.A. Duncan, W. Yang, M. Bär, L. Weinhardt, K. Ramanathan, and C. Heske, ACS Appl. Mater. Interfaces **8**, 33256 (2016).

[2] R. Klenk, A. Steigert, T. Rissom, D. Greiner, C.A. Kaufmann, T. Unold, and M.Ch. Lux-Steiner, Prog. Photovolt: Res. Appl. **22**, 161 (2014).

[3] T. Minemoto, A. Okamoto, and H. Takakura, Thin Solid Films **519**, 7568 (2011).

[4] A. Grimm, D. Kieven, R. Klenk, I. Lauermann, A. Neisser, T. Niesen, and J. Palm, Thin Solid Films **520**, 1330 (2011).

[5] F. Erfurth, A. Grimm, J. Palm, T.P. Niesen, F. Reinert, L. Weinhardt, and E. Umbach, Appl. Phys. Lett. **98**, 142107 (2011).

[6] T. Minemoto, T. Negami, S. Nishiwaki, H. Takakura, and Y. Hamakawa, Thin Solid Films **372**, 4 (2000).

[7] P. Pistor, R. Caballero, D. Hariskos, V. Izquierdo-Roca, R. Wächter, S. Schorr, and R. Klenk, Sol. Energy Mater. Sol. Cells **93**, 148 (2009).

[8] M. Bär, N. Barreau, F. Couzinié-Devy, S. Pookpanratana, J. Klaer, M. Blum, Y. Zhang, W. Yang, J.D. Denlinger, H.-W. Schock, L. Weinhardt, J. Kessler, and C. Heske, Appl. Phys. Lett. **96**, 184101 (2010).

[9] D. Hauschild, F. Meyer, A. Benkert, D. Kreikemeyer-Lorenzo, S. Pohlner, J. Palm, M. Blum, W. Yang, R.G. Wilks, M. Bär, C. Heske, L. Weinhardt, and F. Reinert, J. Phys. Chem. C **119**, 10412 (2015).

[10] D. Hauschild, F. Meyer, A. Benkert, D. Kreikemeyer-Lorenzo, T. Dalibor, J. Palm, M. Blum, W.

Yang, R.G. Wilks, M. Bär, F.T. Reinert, C. Heske, and L. Weinhardt, Prog. Photovolt: Res. Appl. **26**, 359 (2018).

[11] N. Naghavi, S. Spiering, M. Powalla, B. Cavana, and D. Lincot, Prog. Photovolt: Res. Appl. **11**, 437 (2003).

[12] N.A. Allsop, A. Schönmann, H.-J. Muffler, M. Bär, M.C. Lux-Steiner, and Ch.-H. Fischer, Prog. Photovolt: Res. Appl. **13**, 607 (2005).

[13] N. Barreau, J.C. Bernède, S. Marsillac, C. Amory, and W.N. Shafarman, Thin Solid Films **431–432**, 326 (2003).

[14] D. Regesch, L. Gütay, J.K. Larsen, V. Deprédurand, D. Tanaka, Y. Aida, and S. Siebentritt, Appl. Phys. Lett. **101**, 112108 (2012).

[15] W.K. Metzger, I.L. Repins, M. Romero, P. Dippo, M. Contreras, R. Noufi, and D. Levi, Thin Solid Films **517**, 2360 (2009).

[16] A. Kylner, J. Electrochem. Soc. **146**, 1816 (1999).

[17] D. Hauschild, F. Meyer, S. Pohlner, R. Lechner, R. Dietmüller, J. Palm, C. Heske, L. Weinhardt, and F.T. Reinert, J. Appl. Phys. **115**, 183707 (2014).

[18] C. Heske, U. Groh, O. Fuchs, L. Weinhardt, E. Umbach, T. Schedel-Niedrig, C.-H. Fischer, M.C. Lux-Steiner, S. Zweigart, T.P. Niesen, F. Karg, J.D. Denlinger, B. Rude, C. Andrus, and F. Powell, J. Chem. Phys. **119**, 10467 (2003).

[19] C. Heske, U. Groh, L. Weinhardt, O. Fuchs, B. Holder, E. Umbach, C. Bostedt, L.J. Terminello, S. Zweigart, T.P. Niesen, and F. Karg, Appl. Phys. Lett. **81**, 4550 (2002).

[20] A. Loubat, M. Bouttemy, S. Gaiaschi, D. Aureau, M. Frégnaux, D. Mercier, J. Vigneron, P. Chapon, and A. Etcheberry, Thin Solid Films **633**, 87 (2017).

[21] J.R. Vig, C.F. Cook, K. Schwidtal, J.W. Lebus, and E. Hafner, in *28th Annual Symposium on*

Frequency Control (IEEE, Atlantic City, NJ, USA, 1974), pp. 96–108.

[22] J.R. Vig, J.W. Lebus, and R.L. Filler, in *29th Annual Symposium on Frequency Control* (IEEE, Atlantic City, NJ, USA, 1975), pp. 220–229.

[23] J.R. Vig and J. LeBus, IEEE Trans. Parts, Hybrids, Packag. **12**, 365 (1976).

[24] J.R. Vig, J. Vac. Sci. Technol. A **3**, 1027 (1985).

[25] N. Mahmoodi, A.I. Rushdi, J. Bowen, A. Sabouri, C.J. Anthony, P.M. Mendes, and J.A. Preece, J. Vac. Sci. Technol. A **35**, 041514 (2017).

[26] C.-T. Wang, C.-C. Ting, P.-C. Kao, S.-R. Li, and S.-Y. Chu, J. Appl. Phys. **122**, 085501 (2017).

[27] S.Y. Kim, J.-L. Lee, K.-B. Kim, and Y.-H. Tak, J. Appl. Phys. **95**, 2560 (2004).

[28] K. Sugiyama, H. Ishii, Y. Ouchi, and K. Seki, J. Appl. Phys. **87**, 295 (2000).

[29] R.W.C. Hansen and J. Umhoefer, in *AIP Conference Proceedings* (AIP, Stanford, California (USA), 2000), pp. 128–133.

[30] L. Weinhardt, C. Heske, E. Umbach, T.P. Niesen, S. Visbeck, and F. Karg, Appl. Phys. Lett. **84**, 3175 (2004).

[31] D.W. Niles, M. Contreras, K. Ramanathan, and R. Noufi, in *Conference Record of the 25th IEEE Photovoltaic Specialists Conference - 1996* (IEEE, Washington, DC, USA, 1996), pp. 833–836.

[32] C. Heske, R. Fink, E. Umbach, W. Riedl, and F.H. Karg, Cryst. Res. Technol. **31**, 919 (1996).

[33] L. Weinhardt, D. Hauschild, and C. Heske, Adv. Mater. **31**, 1806660 (2019).

[34] J. Palm, V. Probst, and F.H. Karg, Sol. Energy **77**, 757 (2004).

[35] J.F. Moulder, W.F. Stickle, P.E. Sobol, and K.D. Bomben, *Handbook of X-Ray Photoelectron Spectroscopy: A Reference Book of Standard Spectra for Identification and Interpretation of XPS Data* (Perkin-Elmer Corporation, Eden Prairie, Minnesota, 1992).

[36] L. Weinhardt, M. Blum, O. Fuchs, A. Benkert, F. Meyer, M. Bär, J.D. Denlinger, W. Yang, F. Reinert,

and C. Heske, J. Electron Spectrosc. **188**, 111 (2013).

[37] T. Dalibor, S. Jost, H. Vogt, R. Brenning, A. Heiß, S. Visbeck, T. Happ, J. Palm, A. Avellán, T.P. Niesen, and F. Karg, in *25th European Photovoltaic Solar Energy Conference (EPSEC)* (Valencia, Spain, 2010), pp. 2854–2857.

[38] J. Palm, V. Probst, W. Stetter, R. Toelle, S. Visbeck, H. Calwer, T.P. Niesen, H. Vogt, O. Hernández, M. Wendl, and F.H. Karg, Thin Solid Films **451–452**, 544 (2004).

[39] C. Heske, G. Richter, Z. Chen, R. Fink, E. Umbach, W. Riedl, and F. Karg, J. Appl. Phys. **82**, 2411 (1997).

[40] G. Greczynski and L. Hultman, Appl. Surf. Sci. **451**, 99 (2018).

[41] T.L. Barr and S. Seal, J. Vac. Sci. Technol. A **13**, 1239 (1995).

[42] A.V. Naumkin, A. Kraut-Vass, S.W. Gaarenstroom, and C.J. Powell, NIST Standard Reference Database 20, Version 4.1.

[43] C. Heske, R. Fink, E. Umbach, W. Riedl, and F. Karg, Appl. Phys. Lett. **68**, 3431 (1996).

[44] M.C. Biesinger, Surf. Interface Anal. **49**, 1325 (2017).

[45] L. Weinhardt, O. Fuchs, D. Groß, E. Umbach, C. Heske, N.G. Dhere, A.A. Kadam, and S.S. Kulkarni, J. Appl. Phys. **100**, 024907 (2006).

[46] M. Morkel, L. Weinhardt, B. Lohmüller, C. Heske, E. Umbach, W. Riedl, S. Zweigart, and F. Karg, Appl. Phys. Lett. **79**, 4482 (2001).

[47] C. Heske, U. Groh, O. Fuchs, E. Umbach, N. Franco, C. Bostedt, L.J. Terminelo, R.C.C. Perera, K.H. Hallmeier, A. Preobrajenski, R. Szargan, S. Zweigart, W. Riedl, and F. Karg, Phys. Stat. Sol. **187**, 13 (2001).